ARL-TR-9969 ● SEP 2024

Hot-pressing and Characterization of Potassium Sodium Niobate, $(K_{0.5}Na_{0.5})NbO_3$ Incorporated with Tungsten (W-KNN)

by Latha Nataraj and Tucker Moore

NOTICES

Disclaimers

The findings in this report are not to be construed as an official Department of the Army position unless so designated by other authorized documents.

Citation of manufacturer's or trade names does not constitute an official endorsement or approval of the use thereof.

Destroy this report when it is no longer needed. Do not return it to the originator.

ARL-TR-9969 ● SEP 2024

Hot-pressing and Characterization of Potassium Sodium Niobate, $(K_{0.5}Na_{0.5})NbO_3$ Incorporated with Tungsten (W-KNN)

Latha Nataraj and Tucker Moore
DEVCOM Army Research Laboratory

REPORT DOCUMENTATION PAGE

1. REPORT DATE	2. REPORT TYPE	3. DATES COVERED	
		START DATE	END DATE
September 2024	Technical Report	8/1/2023	6/1/2024

4. TITLE AND SUBTITLE
Hot-pressing and Characterization of Potassium Sodium Niobate, $(K_{0.5}Na_{0.5})NbO_3$ Incorporated with Tungsten (W-KNN)

5a. CONTRACT NUMBER	5b. GRANT NUMBER	5c. PROGRAM ELEMENT NUMBER
5d. PROJECT NUMBER	**5e. TASK NUMBER**	**5f. WORK UNIT NUMBER**

6. AUTHOR(S)
Latha Nataraj and Tucker Moore

7. PERFORMING ORGANIZATION NAME(S) AND ADDRESS(ES)	8. PERFORMING ORGANIZATION REPORT NUMBER
DEVCOM Army Research Laboratory ATTN: FCDD-RLA-VB Aberdeen Proving Ground, MD 21005	ARL-TR-9969

9. SPONSORING/MONITORING AGENCY NAME(S) AND ADDRESS(ES)	10. SPONSOR/MONITOR'S ACRONYM(S)	11. SPONSOR/MONITOR'S REPORT NUMBER(S)

12. DISTRIBUTION/AVAILABILITY STATEMENT
DISTRIBUTION STATEMENT A. Approved for public release: distribution unlimited.

13. SUPPLEMENTARY NOTES

ORCIDs: Latha Nataraj, 0000-0001-5041-8809; Tucker Moore, 0009-0000-9646-8465

14. ABSTRACT

Multifunctional potassium sodium niobate, $(K_{0.5}Na_{0.5})NbO_3$ (KNN) has emerged as one of the most promising, lead-free, nontoxic, environment-friendly, and biocompatible candidates to replace high-performing, lead-based piezoelectric materials. It is well known that obtaining phase-pure materials with a high density and a uniform, fine-grained microstructure is a major challenge. In addition, KNN is known for poor densification and an extremely narrow range of sintering temperature (also very close to the solidus temperature) that some studies have attributed to the coarsening of the microstructure without densification, which contributes to a reduction of the driving force for sintering. Here, we report our success at the US Army Combat Capabilities Development Command Army Research Laboratory in developing a tailored hot-pressing technique to obtain well-sintered KNN compacts with high density and characterizing their properties.

15. SUBJECT TERMS
Biological and Biotechnology Sciences; Electromagnetic Spectrum Sciences; Mechanical Sciences; Photonics, Electronics, and Quantum Sciences; Sciences of Extreme Materials, ceramics, sintering, hot-press, lead-free, nontoxic, biocompatible, piezoelectric, multifunctional, potassium sodium niobate

16. SECURITY CLASSIFICATION OF:			17. LIMITATION OF ABSTRACT	18. NUMBER OF PAGES
a. REPORT	b. ABSTRACT	C. THIS PAGE		
UNCLASSIFIED	UNCLASSIFIED	UNCLASSIFIED	UU	29

19a. NAME OF RESPONSIBLE PERSON	19b. PHONE NUMBER *(Include area code)*
Latha Nataraj	(410) 278-3814

STANDARD FORM 298 (REV. 5/2020)
Prescribed by ANSI Std. Z39.18

Contents

List of Figures

1. Introduction

Piezoelectric materials are a vital family of functional materials with a wide array of applications such as sensors, actuators, and transducers, to name a few.[1,2] Lead-based perovskites, predominantly $Pb(Zr,Ti)O_3$ (PZT)-based ceramics, which have excellent electromechanical properties are widely popular for these applications. However, significant concerns to environmental and human safety have resulted in a quest for nonhazardous alternatives over the last couple of decades. Three main groups of materials have emerged as promising alternatives to replace these lead-based materials: $(K_{0.5}Na_{0.}5)NbO_3$ (KNN)-based, $BaTiO_3$ (BT)-based, and $Bi_1/2Na_1/2TiO_3$ (BNT)-based piezoelectric materials.

While it currently seems almost impossible for any one of these materials to fully replace PZT in all applications, many compositions have demonstrated comparable or even better performances for specific requirements. Although these materials were studied as early as the 1950s,[3–5] intensive research only began after 2004 with the discovery of a large piezoelectric response in Li-, Ta-, Sb-modified-and-textured KNN.[6] Good thermal stability of the electromechanical performance[7,8]; high fatigue resistance[9,10] and mechanical characteristics[11,12]; compatibility with low-cost, base-metal electrodes[13]; and biocompatibility[14]; have rendered the multifunctional KNN as significantly advantageous over other lead-free compositions with applications in piezoelectric transformers,[15] knock sensors,[16] multilayer actuators,[17] ultrasonic motors,[18] and ultrasonic transducers.[19]

Despite some demonstrated promising characteristics, KNN-based piezoelectrics are still not widely used in industry. Challenges with obtaining high densities in sintered bulk is one of the most frequently reported drawbacks related to processing, among others,[20–25] which leads to low piezoelectric performance, nonuniform distribution of the applied electric field, leakage current, low breakdown fields, and poor reproducibility of the material. Several underlying mechanisms have been carefully studied to improve sintering characteristics of KNN.

2. Fundamentals of Sintering KNN

Sintering is among the oldest techniques in processing ceramics such as KNN. It is an irreversible thermodynamic process in which powder material is consolidated using thermally activated diffusion to obtain dense, polycrystalline bulk ceramics. The main thermodynamic driving force for sintering is the reduction of the surface-free energy of the particles in the powder. As such, increasing the surface-free energy by reducing particle sizes can promote densification. In addition to the increase in curvature of the particle surface with decreasing particle size, driving force can be increased by applying external pressure or a chemical reaction.[26]

The sintering process may be described as an interplay between densification and grain growth, and may be divided into three overlapping **sintering stages**, based on changes in the grain size and shape, the pore size and shape, and the related densification kinetics.

1) In the first stage, the particles become connected at their contact points by small necks, with a decrease in their surface roughness, and interconnected particles form a porous network with a relative density of 60%–70%.

2) The next stage is characterized by an increased densification rate resulting in rapid shrinkage. The pores gradually diminish and the connections between them disappear, resulting in the "closed-porosity" state (usually at a relative density of 92%–95%).

3) In the third and final stage, the densification rate dramatically decreases, while the isolated pores can either shrink and disappear or merge to grow. This stage is typically characterized by grain growth, which strongly depends on the grain-boundary mobility and the pore/grain-boundary interaction. Also, there could be abnormal grain growth, resulting in an increased number of diffusion paths between the pores and grain boundaries, and entrapment of pores within the large grains. This could prevent material transport toward the pores and, consequently, cease the densification process.

Figure 1 shows the processes in action during solid-state sintering. As shown, material transport occurs across the microstructure, which can take place via lattice diffusion from grain boundary (a), grain-boundary diffusion (b), viscous flow (c), surface diffusion (d), lattice diffusion from the surface to the neck (e), or evaporation/condensation (f). While all these mechanisms promote neck growth, only a–c contribute to the densification (densifying mechanisms), and d–f do not (non-densifying mechanisms).

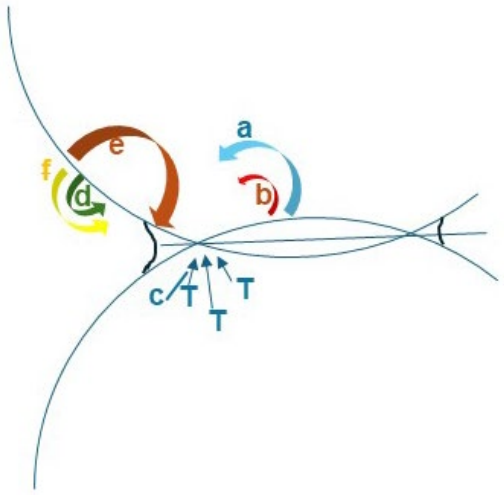

Fig. 1 Material-transport mechanisms during solid-state sintering: lattice diffusion from the grain boundary (a), and from the surface (e) to the neck, grain-boundary diffusion (b), viscous flow (c), surface diffusion (d), and evaporation/condensation (f). The symbol "┬" marks the dislocations and other defects.

The various defects in a polycrystalline material determine the material-transport path via diffusion, as follows:

1) Generally, the activation energy for surface diffusion (*QS*) is expected to be the lowest.

2) Atoms can diffuse along the grain boundaries (disorder between adjacent grains or regions of lattice mismatch) formed during the sintering process. The activation energy for the grain-boundary diffusion (*QGB*) is expected to be as high as *QS*.

3) Diffusion can take place across lattice point defects (vacancies or interstitials), whereby the flux of vacancies should be compensated by the opposite and equal flux of atoms. This mechanism typically has the highest activation energy (*QL*) and is therefore active at higher temperatures.

    a) However, the relationships between the activation energies as previously described should be carefully considered, as demonstrated by several studies.[27]

    b) In addition, several other factors need to be considered while trying to understand the diffusion mechanisms.

4) The fraction of lattice atoms, grain boundaries, and free surfaces change during sintering. This, in turn, changes the contributions from the different mechanisms. Also, the diffusing species in ceramics are generally ions of different and opposite charges (ambipolar diffusion) with different diffusion rates; therefore, one should

be mindful of the impact on the preservation of the stoichiometry and electronegativity.

5) Each ion could have multiple diffusion paths. Diffusion rate is determined by the slowest ion along its fastest path.

6) In addition to the previously mentioned diffusion mechanisms, mass transport can also occur through evaporation/condensation; material transfer is promoted by the difference in vapor pressure between the positive curvature of the particle surface and the negative radius of the neck region. According to the Kelvin equation, vapor pressure. Therefore, the material evaporation/condensation-driven material transport exponentially increases with the increasing particle surface curvature (or decreasing particle size).[28]

The final stage of sintering is when grain growth typically occurs, as illustrated in Fig. 2. The following steps describe the evolution of grain growth.

1) If the average grain size of the material increases continuously with no variations in the grain-size distribution, the growth is considered normal. In this case, atoms diffuse from one side of the grain boundary to the other side with the free-energy difference across the curved grain boundary being the driving force. This results in the grain boundary emerging toward its center of curvature (as represented in the schematic in Fig. 2a).

2) If the grain-boundary energy is isotropic, the balance of the grain-boundary tensions forces the edges to meet at 120°, thereby creating a hexagonal grain with straight sides.

3) Boundaries of the polygons with greater than six sides are concave, while those of polygons with fewer than six sides are convex. As grain boundaries migrate toward their centers of curvature, the grains with convex boundaries tend to shrink, while the ones with concave boundaries tend to grow (Fig. 2b).[29]

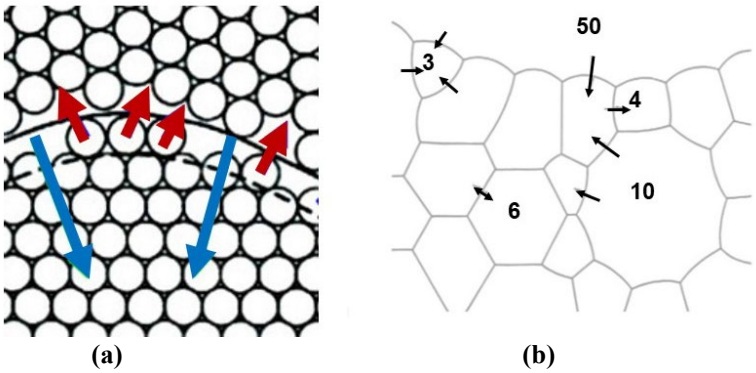

Fig. 2 (a) Movement of the grain boundary toward its center of curvature (blue arrows) by the diffusion of atoms across the boundary (red arrows). (b) Movements of grain boundaries (black arrows) depending on the number of sides in a polycrystalline ceramic.

Specific local conditions such as anisotropic grain-boundary energies and grain-boundary structures,[30,31] preferential segregation of dopants/impurities,[32] and second-phase particles or pores affect grain-boundary mobility causing abnormal grain growth, which results in a bimodal grain-size distribution (i.e., a small fraction of the grains grow unusually quickly to reach a large size in a matrix of fine grains, which grow with a slow rate), and are generally undesirable. Additionally, the presence of a liquid phase or a nonuniform particle/grain-size distribution can also cause abnormal grain growth.[26,33] Also, other factors such as pores affect grain-boundary mobility. A grain boundary moving under the influence of its curvature applies a force on a pore at the boundary, resulting in a change of the pore shape,[34] as in Fig. 3.

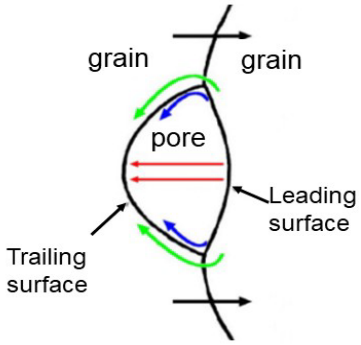

Fig. 3 Schematic of a pore moving with the grain boundary and possible material-transport mechanisms (blue: surface diffusion, green: lattice diffusion, and red: evaporation/condensation)

Material transport can occur through surface diffusion, lattice diffusion, or evaporation/condensation. The different curvatures of the leading and trailing surfaces of the pore create a chemical potential difference driving the atom flux. The number of pores, their mobility, and the intrinsic grain-boundary mobility together determine the overall grain-boundary migration.[35,36] When the grain-boundary-migration velocity becomes greater than pore-migration velocity, it results in pore/boundary separation. It is hard to eliminate the entrapped pores because of the long diffusion distances, which limit densification during sintering.[36]

3. KNN Phase Relations

The $K_{1-x}Na_xNbO_3$ system is a "pseudo-binary" solid solution comprised of the ferroelectric $KNbO_3$ phase and the antiferroelectric $NaNbO_3$ phase (Fig. 4).[22,37] The phases crystallize in the perovskite structure with different symmetries. The ferroelectric region is known to have three temperature-induced transitions, while the antiferroelectric region exhibits the more complex polymorphism.[38–40]

The phase transitions in KNN with a K:Na ratio of 1:1 are as follows (Fig. 4)[22,37,41,42]:

1) rhombohedral ⇔ orthorhombic at 160 °C
2) orthorhombic ⇔ tetragonal at 200 °C
3) tetragonal ⇔ cubic phase at 410 °C

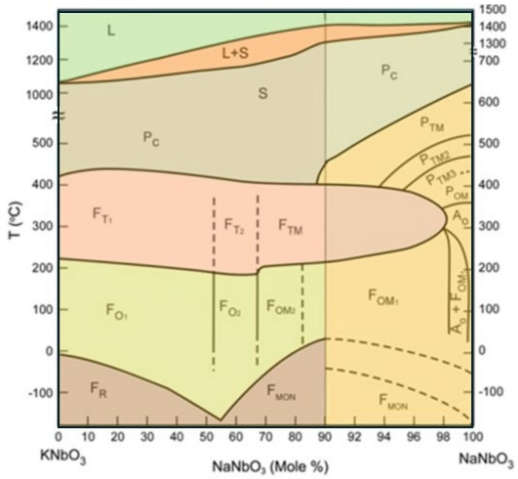

Fig. 4 Phase diagram of the $KNbO_3$–$NaNbO_3$ system showing the phase transitions of $K_{0.5}Na_{0.5}NbO_3$ differential scanning calorimetry (DSC) upon heating

For this composition, the solidus and liquidus lines are at 1140 and 1420 °C, respectively.[37] Studies have suggested that at a K:Na ratio of 1:1, two different orthorhombic phases (O_1 and O_2) coexist, along with the formation of a morphotropic phase boundary (MPB), which is attributed to the enhanced piezoelectric properties.[43] However, it was later demonstrated that there are no symmetry changes in that region.[41] While the room-temperature polymorph of KNN is often described as orthorhombic with space group Amm^2, the perovskite-type ABO_3 primary cell is known to have a monoclinic symmetry[43,44] with lattice parameters $am = cm > bm$. Here, the bm axis is perpendicular to the $amcm$ plane and its inter-axial angle β is slightly larger than 90°.[45] Therefore, while KNN's unit cell has an orthorhombic symmetry at room temperature, the perovskite-type primary cell of KNN is monoclinic.

Doping or the formation of pseudo-binary solid solutions could be used to shift the phase-transition temperatures of KNN materials, which generally result in a downward shift of the orthorhombic–tetragonal phase-transition temperature (TO–T).[7,46–51] The closer the TO–T is to room temperature, the better the piezoelectric performance, also called the polymorphic phase-transition (PPT) effect.[52] It has also been established that modification of KNN compositions using materials as $BaZrO_3$, (Bi,Na,K,)ZrO_3, (Bi,Li)TiO_3, and (Bi,Na)TiO_3, results in an MPB that separates the tetragonal and rhombohedral phases, similar to lead-based piezoelectric materials.[8,53,54]

4. Solid-State Synthesis of Powders

Solid-state synthesis of KNN has been accomplished by reaction of alkali carbonates and niobium oxide,[5] nitrates,[55] hydrogen carbonates,[56] sodium potassium tartrate hydrate,[57] or the two end-member perovskites.[41,58,59] Equation 1 summarizes the reaction of the alkali carbonates and niobium oxide, which occurs between 400 and 700 °C, as determined by thermogravimetric analysis (TGA)[60] with calcination occurring between 750 and 950 °C.

$$K_2CO_3(s) + Na_2CO_3(s) + 2\ Nb_2O_5(s) \rightarrow 4\ K_{0.5}Na_{0.5}NbO_3(s) + 2\ CO_2(g) \quad (1)$$

The reaction proceeds through the coupled diffusion of alkaline and oxygen ions into niobium oxide and the perovskite phase formed after an intermediate alkali polyniobate phase, (K,Na)$2Nb_4O_{11}$. Multiple phases other than the perovskite can be expected to form in these reaction(s).[61–65] Diffusion studies have shown that the potassium ions exhibit a diffusion rate of approximately 1 order of magnitude lower than that of the sodium ions. Therefore, the overall reaction rate in the ternary system is dependent on the diffusion rate and path of the slower potassium ions.[66] Also, as in any diffusion-controlled reaction, smaller particle sizes lead to shorter diffusion paths and lower input energy (heat) for the reaction.[28]

At the US Army Combat Capabilities Development Command Army Research Laboratory (ARL), using the process outlined by Lee et al.[67] as a guideline, we synthesized KNN using a Spex 8000M high-energy mixer/mill. The high-energy ball mill grinds the material in a closed vial with combined back-and-forth swings with short lateral movements, with the ends of the vial forming a figure eight for relatively uniform milling. K_2CO_3, Na_2CO_3, and Nb_2O_5 were mixed in the stoichiometric ratio and dry-milled using a tungsten carbide (WC) vial and milling media. All powders were stored, weighed, and loaded into the vial inside the glovebox, in an argon atmosphere.

TGA and DSC were performed to determine the right calcination temperature and duration to form KNN as the temperature quoted in the process we followed resulted in charred powder. TGA/DSC of the 1-h milled powder determined the calcination temperature to be around 650 °C at completion of the reaction, which is lower than the approximately

850 °C temperature found in other processes.[67,68] The resulting powder mixture from the milling process was then calcined at a temperature of 650 °C for 1 h to complete the mechanochemical reaction to achieve KNN. The structural characteristics of the calcined powders were then studied using X-ray diffraction (XRD), scanning electron microscopy (SEM), energy-dispersive X-ray, transmission electron microscopy, and energy dispersive X-ray spectroscopy. More details on the KNN synthesis and basic material characterization may be found in our earlier publication.[69]

Alkali deficiency has been a common problem with KNN synthesis and is attributed to the hygroscopicity K_2CO_3 resulting in polyniobate phases, which are hygroscopic even at room temperature.[70] Inert and dry environments for KNN synthesis and processing,[58] using a slight excess of alkali compounds in the reagent mixture,[13] and additional extended heating steps[71] have been approaches employed to overcome this issue. The KNN synthesized in this work has demonstrated incorporation of a small amount of W and an Nb-deficiency[69]; the impact of these on bulk characteristics and performance is currently being investigated.

5. Solid-State Sintering of KNN

Poor densification has been a main problem preventing the widespread application of KNN-based piezoceramics. Few systematic reports on the sintering of these materials can be found in the literature. Section 6 summarizes the existing knowledge about the processes occurring during the solid-state sintering of alkaline niobates—such as, material-transport mechanisms, microstructure development, and grain growth.

6. Sintering Mechanisms

Sintering mechanisms in complex oxides, such as KNN, are challenging to study due to the volatile oxides,[71] anisotropy of the surface energy,[72,73] ambipolar diffusion,[66]—and potentially, multiple simultaneous diffusion mechanisms in play. Conventional high-temperature processing with uniaxial pressure might result in low density, perhaps due to evaporation of sodium, sintering-induced alkali vacancies and lack of liquid phase in the microstructure of pure KNN.[74–77] To improve density and performance of KNN, researchers have tried low-oxygen partial pressure processes[78,79] to suppress the formation of vacancies and reduce interaction with oxygen, using H_2 or Ar atmospheres,[80] sealed sintering (which greatly improved density and electrical properties),[81] spark plasma sintering (which provided high improvements although technologically very demanding),[82] and the addition of various dopants,[6,46,57,83–85] rare earth metal oxides,[86] and liquid-phase sintering.[87]

The synthesized KNN powder was made into a compact using the hot-pressing technique as the process renders samples with improved density of the resulting compacts compared

to commonly used techniques. Also, hot-pressing promotes texturization of the microstructure by the uniaxial pressing enhancing directed grain growth during sintering, which is desirable for piezoelectric applications.[88] Moreover, the reduced sintering temperature may reduce the overall alkali evaporation, allowing better control over the material stoichiometry.

Following multiple experimental trials involving pressing and sintering at varying temperatures, we successfully established hot-pressing methods available in ARL's Ceramics and Transparent Materials Branch. These methods were further enhanced through the process outlined by Rutkowski et al.[74] First, approximately 2 g of the synthesized W-KNN powder with 60-min milling time was weighed out. A 1-inch-diameter cylindrical graphite die was coated uniformly with a slurry of hexagonal–boron nitride (h-BN) and ethyl alcohol to act as a diffusion barrier for carbon between the graphite die and the part during hot-pressing. Bharathi and Varma[43] demonstrated that h-BN helps with the stimulation of the KNN densification process. After placing the coated die in an oven at 70 °C for 1 h to evaporate any traces of ethyl alcohol from the coating, the W-KNN powder was placed between BN spacers, pressed with 8000 lbf three times, and held for 10 s each time to obtain a robust green compact. This was then transferred to an Oxygon benchtop refractory-metal-hot-press, which uses tungsten elements and tungsten/ molybdenum heat shields, with graphite pressing rams. The system was evacuated to 10^{-5} torr, then backfilled with gettered ultra-high purity Ar (<1 ppb O_2). The die was heated at 50 °C/min to temperatures from 700 to 900 °C, held at this temperature for 1 h, and then cooled at 50 °C/min to room temperature. A uniaxial load of 8000 lbf (70.3 MPa) was applied for the duration of the 1-h hold.

The hot-pressed W-KNN discs were well sintered and robust as shown in Fig. 5. The density of the three samples as measured by gas pycnometry are given as a function of process temperature in Fig. 6. The sample was hot-pressed at 800 °C and showed the highest relative density at 95.8%. At 700 °C this value is slightly reduced, which is expected when lowering sintering temperatures. However, at 900 °C, the density is again reduced. This may be due to partial vaporization of the alkalis generating pores, and changes in stoichiometry affecting diffusivity.

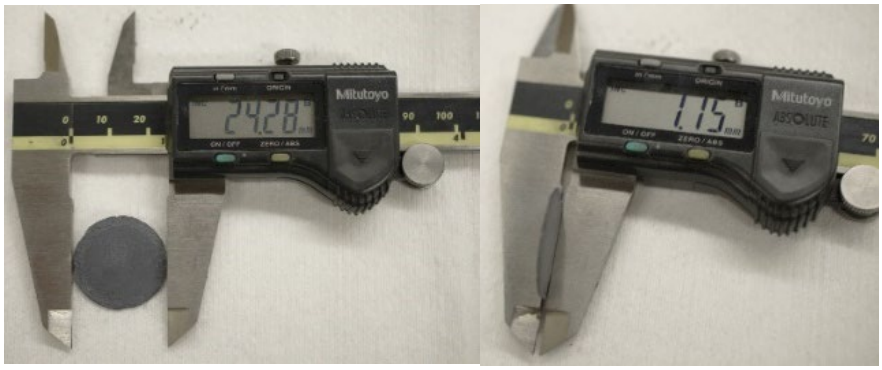

Fig. 5 Well-sintered, dense compact made with synthesized W-KNN powder hot-pressed at 800 °C: (left) diameter, (right) thickness

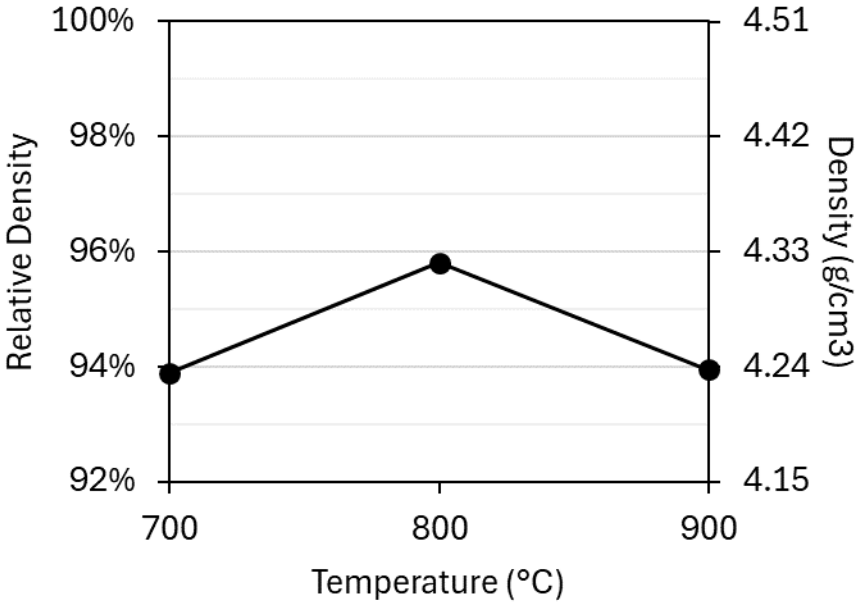

Fig. 6 Measured densities of W-KNN samples hot-pressed at different temperatures

To ensure that the phase content of the powder had not changed due to the processing schedule, XRD measurements were taken of the starting powder and each of the three hot-pressed samples (Fig.7). These data show that the starting powder is phase pure and remains as such after sintering.

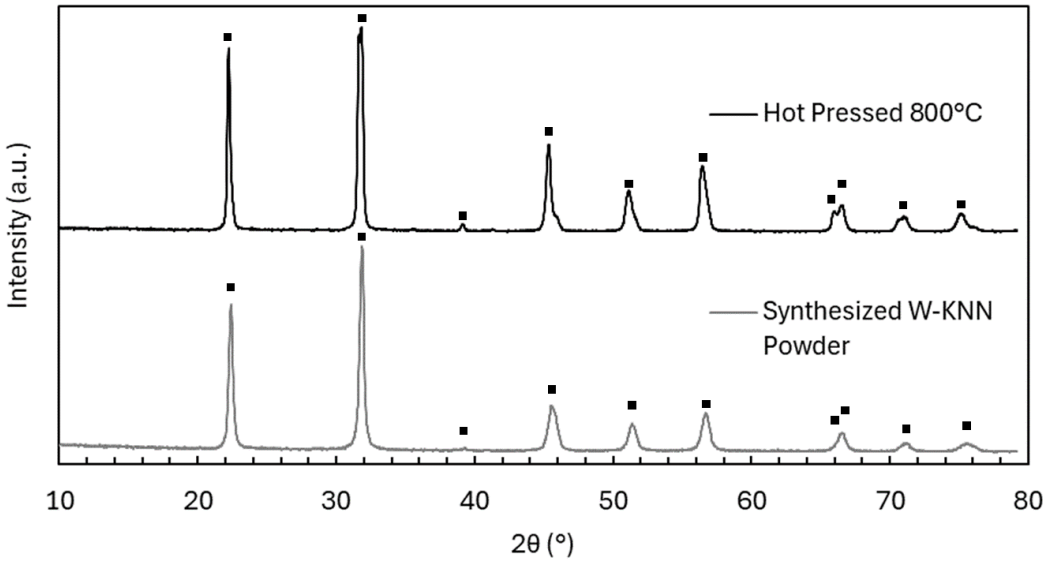

Fig. 7 XRD plot of the synthesized KNN powder and the sample hot-pressed at 900 °C

A cross section of the 800 °C sample was polished to a 0.25-µm finish using diamond impregnated grinding pads and diamond slurries. After polishing, the samples were analyzed using a PhenomXL SEM at 15 kV using the solid-state backscatter detector. Representative microstructures of the sample are given in Fig. 8. The sample has very fine grains, typically <1 µm. The starting powder had a d_{50} particle size of 0.78 µm, which indicates remarkably little grain growth. There is a small amount of porosity evident throughout the sample, typical of sintered ceramic microstructures. Using the Intermodes thresholding algorithm in imageJ, the porosity level was measured to be 3.4%, which is in line with the density measurement of 4.2%.

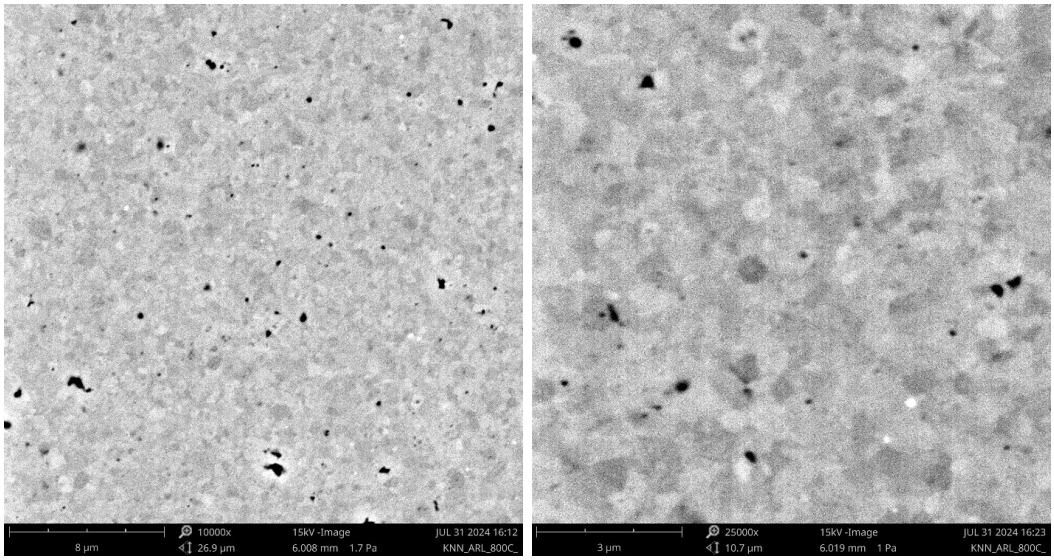

Fig. 8 SEM micrographs of the W-KNN sample hot-pressed at 900 °C

Energy-dispersive spectroscopy (EDS) measurements of the starting powder and hot-pressed sample were used as an estimate of alkali loss from evaporation (Fig. 9). The powder had a K:Na atomic ratio of 1.62:1, and after hot-pressing, the K:Na lowered to 1.57:1. As previously shown in other systems, this is likely due to Na vaporization at high temperatures. Further analysis on samples pressed at different temperatures with this process is underway.

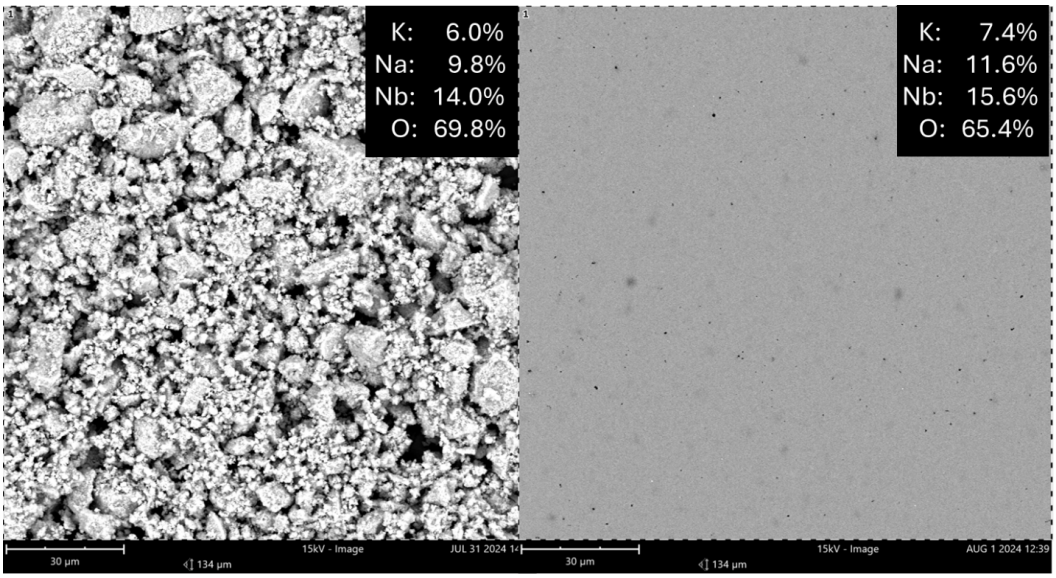

Fig. 9 SEM field of view and EDS measurements for W-KNN powder (left) and W-KNN hot-pressed at 800 °C (right)

The color of the discs is dramatically different from the starting powder, having changed from a white powder to a dark gray. This is likely due to a mixture of C diffusion into the sample, as well as O_2 vacancies created due to reactions between the powder and C, as well as the O_2-free atmosphere.[89] These defects may affect the piezoelectric performance of the hot-pressed samples; therefore, further investigation is being performed to anneal the sintered parts in air to reintroduce O to the lattice.

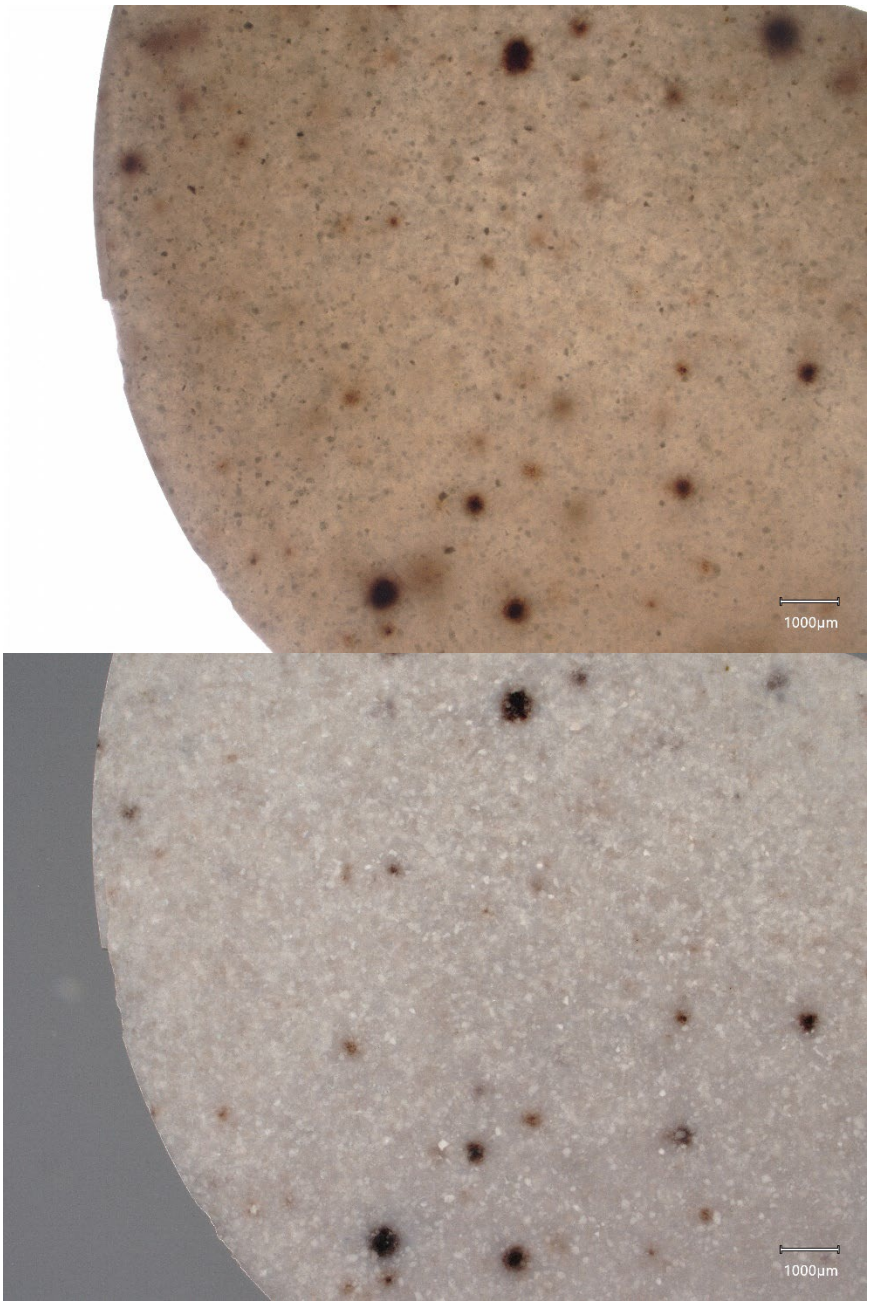

Fig. 10 Optical micrographs of the sample hot-pressed in an alumina die, shown using a transmission light source (top) and reflection light source (bottom)

To minimize the effect of C contamination, an additional experiment was conducted on a commercial KNN powder (American Elements). Essentially, the same hot-pressing technique was used, but aluminum-oxide die and punches were used in place of the BN-coated graphite. It was supposed that this change should lead to reduced C diffusion into the sample (although some is still possible due to the graphite rams), and may also reduce the concentration of O_2 vacancies due to the increased partial pressure of O and lowered partial pressure of C within the die. Due to the lowered thermal conductivity of aluminum

oxide compared to graphite, the heating rate was lowered to 10 °C/min to minimize thermal gradients. After hot-pressing, extracting the sample was much more difficult than is typical with graphite dies. As graphite is naturally lubricious, the punches can usually move relatively freely even with tight tolerances between the punches and inner die wall. With the aluminum-oxide die, the punches became stuck after hot-pressing and had to be hammered out to loosen them. However, the sample inside remained intact. In contrast to the samples made with graphite dies, this one remained mostly white, with some dark spots on the surface as seen in Fig. 10. After polishing, it was noted that the sample is translucent, save for the dark spots. These spots are likely due to impurities in the commercial powder, but could also be due to C contamination from the hot-press. Further investigation of this process using the W-KNN powder is underway.

7. Conclusions

A tailored hot-pressing technique to obtain well-sintered W-KNN compacts with high density has been developed. The sintered compacts have been characterized for structural integrity. While these well-sintered dense compacts are being characterized for various functionalities afforded by KNN (piezoelectric, thermoelectric, optical, nonlinear photonic), more research is underway to fine-tune this process to obtain purer bulk W-KNN samples.

8. References

1. Setter N. Piezoelectric materials in devices. EPFL Swiss Federal Institute of Technology; 2002.
2. Malič B, Koruza J, Hreščak J, Bernard J, Wang K, Fisher JG, Benčan A. Sintering of lead-free piezoelectric sodium potassium niobate ceramics. Materials. 2015;8:8117–8146.
3. Matthias BT, Remeika JP. Dielectric properties of sodium and potassium niobates. Phys Rev. 1951;82L727–729.
4. Shirane G, Newnham R, Pepinsky R. Dielectric properties and phase transitions of $NaNbO_3$ and $(Na,K)NbO_3$. Phys Rev. 1954;96:581–588.
5. Egerton L, Dillon DM. Piezoelectric and dielectric properties of ceramics in the system potassium-sodium niobate. J Am Ceram Soc. 1959;42:438–442.
6. Saito Y, Takao H, Tani T, Nonoyama T, Takatori K, Homma T, Nagaya T, Nakamura M. Lead-free piezoceramics. Nature. 2004;432:84–87.
7. Wang K, Yao F-Z, Jo W, Gobeljic D, Shvartsman VV, Lupascu DC, Li J-F, Rödel J. Temperature-insensitive $(K,Na)NbO_3$-based lead-free piezoactuator ceramics. Adv Funct Mater. 2013;4079–4086.
8. Wang R, Wang K, Yao F-Z, Li J-F, Schader FH, Webber KG, Jo W, Rödel J. Temperature stability of lead-free niobate piezoceramics with engineered morphotropic phase boundary. J Am Ceram Soc. 2015;98:2177–2182.
9. Yao FZ, Patterson EA, Wang K, Jo W, Rodel J, Li JF. Enhanced bipolar fatigue resistance in $CaZrO_3$-modified (K,Na) NbO_3 lead-free piezoceramics. Appl Phys Lett. 2014;104.
10. Yao F-Z, Wang K, Shen Y, Li J-F. Robust CaZrO3-modified $(K,Na)NbO_3$-based lead-free piezoceramics: high fatigue resistance insensitive to temperature and electric field. J Appl Phys. 2015;118.
11. Park BC, Hong IK, Jang HD, Tran VDN, Tai WP, Lee JS. Highly enhanced mechanical quality factor in lead-free $(K_{0.5}Na_{0.5})NbO_3$ piezoelectric ceramics by co-doping with $K_{5.4}Cu_{1.3}Ta_{10}O_{29}$ and CuO. Mater Lett. 2010;64:1577–1579.
12. Gurdal EA, Ural SO, Park HY, Nahm S, Uchino K. High power $(Na_{0.5}K_{0.5})NbO_3$-based lead-free piezoelectric transformer. Jpn J Appl Phys. 2011;50.

13. Kawada S, Kimura M, Higuchi Y, Takagi H. (K,Na)NbO_3-based multilayer piezoelectric ceramics with nickel inner electrodes. Appl Phys Express. 2009;2:111401.

14. Nilsson K, Lidman J, Ljungstrom K, Kjellman, inventors; St Jude Medical AB, assignee. Biocompatible material for implants. United States patent US 6,526,984 B1. 2003 Mar 4.

15. Guo M, Lam KH, Lin DM, Wang S, Kwok KW, Chan HLW, Zhao XZ. A Rosen-type piezoelectric transformer employing lead-free K0.5Na0.5NbO_3 ceramics. J Mater Sci. 2008;43:709–714.

16. Non-resonant type knock sensor. Niterra Co, Ltd; (n.d.) [accessed 2015 Jan 10]. https://www.ngkntk.co.jp/english/product/sensors_plugs/knock.html.

17. Kobayashi K, Doshida Y, Mizuno Y, Randall CA. Possibility of cofiring a nickel inner electrode in a ($Na_{0.5}K_{0.5}$)NbO_3–LiF piezoelectric actuator. Jpn J Appl Phys. 2013;52:09KD07.

18. Hong C-H, Han H-S, Lee J-S, Wang K, Yao F-Z, Li J-F, Gwon J-H, Quyet NV, Jung J-K, Jo W. Ring-type rotary ultrasonic motor using lead-free ceramics. J Sens Sci Technol. 2015;24:228–231.

19. Bantignies C, Filoux C, Mauchamp P, Dufait R, Pham Thi M, Rouffaud R, Gregoire JM, Levassort F. Lead-free high-frequency linear-array transducer (30 MHz) for in vivo skin imaging. Proceedings of IEEE International Ultrasonics Symposium; 2013 July 21–25; Prague, Czech Republic. p. 785–788.

20. Malic B, Bencan A, Rojac T, Kosec M. Lead-free piezoelectrics based on alkaline niobates: Synthesis, sintering and microstructure. Acta Chim Slov. 2008;55:719–726.

21. Priya S, Nahm S. Lead-free piezoelectrics. Springer; 2012.

22. Jaffe B, Cook WR, Jaffe H. Piezoelectric ceramics. Academic Press; 1971.

23. Acker J, Kungl H, Hoffmann MJ. Influence of alkaline and niobium excess on sintering and microstructure of sodium-potassium Niobate ($K_{0.5}Na_{0.5}$)NbO_3. J Am Ceram Soc. 2010;93:1270–1281.

24. Wang Y, Damjanovic D, Klein N, Hollenstein E, Setter N. Compositional inhomogeneity in Li- and Ta-modified (K,Na)NbO_3 ceramics. J Am Ceram Soc. 2007;90:3485–3489.

25. Rojac T, Benčan A, Uršič H, Malič B, Kosec M. Synthesis of a Li- and Ta-modified (K,Na)NbO_3 solid solution by mechanochemical activation. J Am Ceram Soc. 2008;91:3789–3791.

26. Rahaman MN. Ceramic processing and sintering. 2nd ed. Marcel Dekker; 2003.

27. German RM. Sintering theory and practice. John Wiley & Sons, Inc; 1996.

28. Kingery WD, Bowen HK, Uhlmann DR. Introduction to ceramics. John Wiley & Sons, Inc; 1976.

29. Burke JE. The development of pore-free ceramics. Sintering Key Papers. In: Somiya S, Moriyoshi Y, editors. Elsevier Science Publishing; 1989. p. 3–17.

30. Rollett AD, Srolovitz DJ, Anderson MP. Simulation and theory of abnormal grain growth—anisotropic grain boundary energies and mobilities. Acta Metall. 1989;37:1227–1240.

31. Lee BK, Chung SY, Kang SJL. Grain boundary faceting and abnormal grain growth in $BaTiO_3$. Acta Mater. 2000;48:1575–1580.

32. Horn DS, Messing GL. Anisotropic grain growth in TiO_2-doped alumina. Mater Sci. Eng A. 1995;195:169–178.

33. Bateman CA, Bennison SJ, Harmer MP. Mechanism for the role of magnesia in the sintering of alumina containing small amounts of a liquid phase. J Am Ceram Soc. 1989;72:1241–1244.

34. Hsueh CH, Evans AG, Coble RL. Microstructure development during final intermediate stage sintering—I. Pore grain-boundary separation. Acta Metall. 1982;30:1269–1279.

35. Nichols FA. Further comments on the theory of grain growth in porous compacts. J Am Ceram Soc. 1968;51:468.

36. Brook RJ. Pore-grain boundary interactions and grain growth. J Am Ceram Soc. 1969;52:56–57.

37. Li J-F, Wang K, Zhu F-Y, Cheng L-Q, Yao F-Z. $(K,Na)NbO_3$-based lead-free piezoceramics: Fundamental aspects, processing technologies, and remaining challenges. J Am Ceram Soc. 2013;96:3677–3696.

38. Tennery VJ. High-temperature phase transitions in $NaNbO_3$. J Am Ceram Soc. 1965;48:537–539.

39. Megaw HD. 7 phases of sodium niobate. Ferroelectrics. 1974;7:87–89.

40. Koruza J, Tellier J, Malič B, Bobnar V, Kosec M. Phase transitions of sodium niobate powder and ceramics, prepared by solid state synthesis. J Appl Phys. 2010;108:113509.

41. Tellier J, Malic B, Dkhil B, Jenko D, Cilensek J, Kosec M. Crystal structure and phase transitions of sodium potassium niobate perovskites. Solid State Sci. 2009;11:320–324.

42. Malic B, Razpotnik H, Koruza J, Kokalj S, Cilensek J, Kosec M. Linear thermal expansion of lead-free piezoelectric $K_{0.5}Na_{0.5}NbO_3$ ceramics in a wide temperature range. J Am Ceram Soc. 2011;94:2273–2275.

43. Tennery VJ, Hang KW. Thermal and X-ray diffraction studies of $NaNbO_3$-$KNbO_3$ system. J Appl Phys. 1968;39:4749–4753.

44. Li J-F, Wang K, Zhang B-P, Zhang L-M. Ferroelectric and piezoelectric properties of fine-grained $Na_{0.5}K_{0.5}NbO_3$ lead-free piezoelectric ceramics prepared by spark plasma sintering. J Am Ceram Soc. 2006;89:706–709.

45. Wang K, Li J-F. Analysis of crystallographic evolution in (Na,K)NbO_3-based lead-free piezoceramics by X-ray diffraction. Appl Phys Lett. 2007;91.

46. Guo YP, Kakimoto K, Ohsato H. $(Na_{0.5}K_{0.5})NbO_3$-$LiTaO_3$ lead-free piezoelectric ceramics. Mater Lett. 2005;59:241–244.

47. Hollenstein E, Davis M, Damjanovic D, Setter N. Piezoelectric properties of Li- and Ta-modified $(K_{0.5}Na_{0.5})NbO_3$ ceramics. Appl Phys Lett. 2005;87.

48. Wang K, Li J-F. Domain engineering of lead-free Li-modified (K,Na)NbO_3 polycrystals with highly enhanced piezoelectricity. Adv Funct Mater. 2010;20:1924–1929.

49. Park HY, Ahn CW, Song HC, Lee JH, Nahm S, Uchino K, Lee HG, Lee HJ. Microstructure and piezoelectric properties of 0.95 $(Na_{0.5}K_{0.5})NbO_3$-$0.05BaTiO_3$ ceramics. Appl Phys Lett. 2006;89.

50. Park HY, Cho KH, Paik DS, Nahm S, Lee HG, Kim DH. Microstructure and piezoelectric properties of lead-free (1-x)$(Na_{0.5}K_{0.5})NbO_3$-x$CaTiO_3$ ceramics. J Appl Phys. 2007;102:124101.

51. Zhou J-J, Wang K, Li F, Li J-F, Zhang X-W, Wang Q-M. High and frequency-insensitive converse piezoelectric coefficient obtained in $AgSbO_3$-modified (Li,K,Na)(Nb,Ta)O_3 lead-free piezoceramics. J Am Ceram Soc. 2013;96:519–523.

52. Dai YJ, Zhang XW, Chen KP. Morphotropic phase boundary and electrical properties of K1-xNaxNbO3 lead-free ceramics. Appl Phys Lett. 2009;94:042905.

53. Tomoaki K, Tsunehiro K, Kazuhiro Y, Subaru M, Masatoshi A. Morphotropic phase boundary slope of (K,Na,Li)NbO_3–$BaZrO_3$ binary system adjusted using third component (Bi,Na)TiO_3 additive. Jpn J Appl Phys. 2013;52:09KD11.

54. Wang X, Wu J, Xiao D, Zhu J, Cheng X, Zheng T, Zhang B, Lou X. Giant piezoelectricity in potassium-sodium niobate lead-free ceramics. J Am Ceram Soc. 2014;136:2905–2910.

55. Powell BRJ. Processing of sodium potassium niobate ceramics [master's thesis]. University of California; 1971.

56. Matsubara M, Yamaguchi T, Kikuta K, Hirano S. Sinterability and piezoelectric properties of (K,Na)NbO_3 ceramics with novel sintering aid. Jpn J Appl Phys. 2004;43:7159–7163.

57. Malic B, Bernard J, Holc J, Jenko D, Kosec M. Alkaline-earth doping in (K,Na)NbO_3 based piezoceramics. J Eur Ceram Soc. 2005;25:2707–271.

58. Hagh NM, Jadidian B, Safari A. Property-processing relationship in lead-free (K,Na,Li) NbO_3-solid solution system. J Electr. 2007;18:339–346.

59. Malic B, Bernard J, Bencan A, Kosec M. Influence of zirconia addition on the microstructure of $K_{0.5}Na_{0.5}NbO_3$ ceramics. J Eur Ceram Soc. 2008;28:1191–1196.

60. Malic B, Jenko D, Bernard J, Cilensek J, Kosec M. Synthesis and sintering of (K,Na)NbO_3 based ceramics. Proceedings of the 2002 Materials Research Society (MRS) Fall Meeting & Exhibit; 2002 Dec 2–5; Boston, MA.

61. Shafer MW, Roy R. Phase equilibria in the system Na_2O-Nb_2O_5. J Am Ceram Soc. 1959;42:482–486.

62. Appendino P. Contributo allo studio del sistema Na_2O-Nb_2O_5. Ann di Chim. 1973;63:547–556.

63. Irle E, Blachnik R, Gather B. The phase diagrams of Na_2O and K_2O with Nb_2O_5 and the ternary system Nb_2O_5-Na_2O-Yb_2O_3. Thermochim Acta. 1991;179:157–169.

64. Reisman A, Holtzberg F. Phase equilibria in the system K_2CO_3-Nb_2O_5 by the method of differential thermal analysis. J Am Chem Soc. 1955;77:2115–2119.

65. Montorsi M, Appendino P, Vallino M. Solid-state equilibria in system niobium pentoxide and lithium and strontium metaniobates. Ann Chim. 1976;66:233–240.

66. Malic B, Jenko D, Holc J, Hrovat M, Kosec M. Synthesis of sodium potassium niobate: a diffusion couples study. J Am Ceram Soc. 2008;91:1916–1922.

67. Lee G-J, Park E-K, Yang S-A, Park J-J, Bu S-D, Lee M-K. Rapid and direct synthesis of complex perovskite oxides through a highly energetic planetary milling. Sci Rep. 2017;7:46241.

68. Quintero MC, Rincón M, Osorio-Guillén JM, López D, Londoño FA. Grinding methods effects on the synthesis of potassium sodium niobate powders by oxide mixing. TecnoLógicas. 2019;22(46):15–23.

69. Nataraj L, Roberts A, Walck S, Moore T, Darling K. Solvent-free mechanochemical synthesis of lead-free piezoelectric perovskite potassium sodium niobate incorporated with tungsten. DEVCOM Army Research Laboratory (US); 2024. Report No.: ARL-TN-1199.

70. Bizeto MA, Constantino VRL. Structural aspects and thermal behavior of the proton-exchanged layered niobate $K_4Nb_6O_{17}$. Mater Res Bull. 2004;39:1729–1736.

71. Popovič A, Bencze L, Koruza J, Maliča B. Vapour pressure and mixing thermodynamic properties of the $KNbO_3$-$NaNbO_3$ system. RSC Adv. 2015;5:76249–76256.

72. Cho CR, Grishin A. Background oxygen effects on pulsed laser deposited Na0.5K0.5NbO3 films: From superparaelectric state to ferroelectricity. J Appl Phys. 2000;87:4439–4448.

73. Kupec A, Malic B, Tellier J, Tchernychova E, Glinsek S, Kosec M. Lead-free ferroelectric potassium sodium niobate thin films from solution: composition and structure. J Am Ceram Soc. 2012;95:515–523.

74. Rutkowski P, Huebner J, Graboś A, Kata D, Sapiński B, Faryna M. Dense KNN polycrystals doped by Er_2O_3 obtained by hot pressing with hexagonal boron nitride protective layer. Materials. 2020.

75. Wang Y, Damjanovic D, Klein N, Setter N. High-temperature instability of Li- and Ta-modified(K,Na)NbO_3 piezoceramics. J Am Ceram Soc. 2008;91:1962–1970.

76. Ichiki M, Zhang L, Tanaka M, Maeda R. Electrical properties of piezoelectric sodium-potassium niobate. J Eur Ceram Soc. 2004;24:1693–1697.

77. Malic B, Koruza J, Hreščak J, Bernard J, Wang K, Fisher JG, Benčan A. Sintering of lead-free piezoelectric sodium potassium niobate ceramics. Materials. 2015;8:8117–8146.

78. Shimizu H, Kobayashi K, Mizuno Y, Randall CA. Advantages of low partial pressure of oxygen processing of alkali niobate: $NaNbO_3$. J Am Ceram Soc. 2014;97:1791–1796.

79. Kobayashi K, Doshida Y, Mizuno Y, Randall CA. A route forwards to narrow the performance gap between PZT and lead-free piezoelectric ceramic with low oxygen partial pressure processed $(Na_{0.5}K_{0.5})NbO_3$. J Am Ceram Soc. 2012;95:2928–2933.

80. Fisher JG, Rout D, Moon KS, Kang SJL. High-temperature X-ray diffraction and Raman spectroscopy study of $(K_{0.5}Na_{0.5})NbO_3$ ceramics sintered in oxidizing and reducing atmospheres. Mater Chem Phys. 2010;120:263–271.

81. Yang D, Ma C, Yang Z, Wei L, Chao X, Yang Z, Yang J. Optical and electrical properties of pressureless sintered transparent $(K_{0.37}Na_{0.63})NbO_3$-based ceramics. Ceram Int. 2016;42:4648–4657.

82. Wei H, Wang H, Xia Y, Cui D, Shi Y, Dong M, Liu C, Ding T, Zhang J-X, Ma Y, et al. An overview of lead-free piezoelectric materials and devices. J Mater Chem C. 2018;6:12446–12467.

83. Zang GZ, Wang JF, Chen HC, Su WB, Wang CM, Qi P, Ming BQ, Du J, Zheng LM, Zhang S, et al. Perovskite $(Na_{0.5}K_{0.5})_{1-x}(LiSb)_x Nb_{1-x} O_3$ lead-free piezoceramics. Appl Phys Lett. 2006;88:212908.

84. Zuo R, Rodel J, Chen R, Li L. Sintering and electrical properties of lead-free $Na_{0.5}K_{0.5}NbO_3$ piezoelectric ceramics. J Am Ceram Soc. 2006;89:2010–2015.

85. Rutkowski P, Huebner J, Graboś A, Kata D, Grzybek D, Sapiński B. Standard hot pressing as a possible solution to obtain dense $K_{0.5}Na_{0.5}NbO_3$ ceramic doped by Er_2O_3 and Yb_2O_3. Materials. 2019;12:4171.

86. Ryu J, Kim HW, Uchino K, Lee J. Effect of Yb addition on the sintering behavior and high power piezoelectric properties of $Pb(Zr,Ti)O_3$–$Pb(Mn,Nb)O_3$. Jpn J Appl Phys. 2003;42:1307–1310.

87. Zhao P, Zhang BP, Li JF. Enhanced dielectric and piezoelectric properties in $LiTaO_3$-doped lead-free $(K,Na)NbO_3$ ceramics by optimizing sintering temperature. Scr Mater. 2008;58:429–432.

88. Roedel J, Jo W, Seifert KTP, Anton EM, Granzow T, Damjanovic D. Perspective on the development of lead-free piezoceramics. J Am Ceram Soc. 2009;92:1153–1177.

89. Schlup AP, Costakis WJ, Rheinheimer W, Trice RW, Youngblood JP. Hot-pressing platelet alumina to transparency. J Am Ceram Soc. 2019;103(4):2587–2601.

List of Symbols, Abbreviations, and Acronyms

ARL	Army Research Laboratory
BNT	$Bi_1/2Na_1/2TiO_3$
BT	$BaTiO_3$
DEVCOM	US Army Combat Capabilities Development Command
DSC	differential scanning calorimetry
EDS	energy-dispersive spectroscopy
h-BN	hexagonal–boron nitride
KNN	potassium sodium niobate; $(K_{0.5}Na_{0.5})NbO_3$
MPB	morphotropic phase boundary
PPT	polymorphic phase-transition
PZT	$Pb(Zr,Ti)O_3$
SEM	scanning electron microscopy
TGA	thermogravimetric analysis
TO–T	orthorhombic–tetragonal phase-transition temperature
WC	tungsten carbide
W-KNN	potassium sodium niobate; $(K_{0.5}Na_{0.5})NbO_3$ incorporated with tungsten
XRD	X-ray diffraction

1 (PDF)	DEFENSE TECHNICAL INFORMATION CTR DTIC OCA
1 (PDF)	DEVCOM ARL FCDD RLB CI TECH LIB